

## **COMPUTER MODELING OF CORROSION IN ABSORPTION COOLING CYCLES**

Andrzej Anderko and Robert D. Young  
OLI Systems Inc.  
108 American Road  
Morris Plains, NJ 07950

### **ABSTRACT**

A comprehensive model has been developed for the computation of corrosion rates of carbon steels in the presence of lithium bromide-based brines that are used as working fluids for absorption refrigeration cycles. The model combines a thermodynamic model that provides realistic speciation of aqueous systems with an electrochemical model for partial cathodic and anodic processes on the metal surface. The electrochemical model includes the adsorption of halides, which strongly influences the corrosion process. Also, the model takes into account the formation of passive films, which become important at high temperatures, at which the refrigeration equipment operates. The model has been verified by comparing calculated corrosion rates with laboratory data for carbon steels in LiBr solutions. Good agreement between the calculated and experimental corrosion rates has been obtained. In particular, the model is capable of reproducing the effects of changes in alkalinity and molybdate concentration on the rates of general corrosion. The model has been incorporated into a program that makes it possible to analyze the effects of various conditions such as temperature, pressure, solution composition or flow velocity on corrosion rates.

**KEY WORDS:** modeling, prediction, thermodynamics, electrochemical kinetics, lithium bromide, molybdate, refrigeration

### **INTRODUCTION**

Refrigeration technology extensively utilizes lithium bromide-based brines as working fluids. Concentrated LiBr solutions have desirable properties as absorbents because of their high hydration heat, high solubility of solid phases, good thermal stability and appropriate viscosity<sup>1</sup>. However, LiBr solutions can cause significant corrosion of construction materials.<sup>2,3</sup> In particular, corrosion problems are exacerbated by the recent trend toward using triple-effect technology, which involves the use of higher temperatures and more corrosive salts in addition to LiBr<sup>1</sup>. The main practical problem associated with corrosion is the evolution of hydrogen, which impairs the efficiency of the cooling cycles if preventive measures are not taken. The hydrogen evolution is a direct result of general corrosion of steel. Thus, it is necessary to use protection techniques such as pH control, application of inhibitors or inorganic coatings to minimize general corrosion.

The rate of corrosion in refrigeration cycles is determined by a multitude of factors such as temperature, concentration of the working fluid, pH, the presence of additional components, flow conditions and metallurgical factors. Thus, it is desirable to develop a model that would reproduce the effect of these factors on corrosion rates and, as a result, save the cost of performing numerous experiments.

The working fluids are frequently multicomponent systems that include pH-adjusting agents and inhibitors. Therefore, it is desirable to incorporate the full chemistry of the working fluids into the model. For this purpose, it is evident that the model should include both thermophysical and electrochemical modules. The thermophysical module should predict the full speciation, activities of all species and phase equilibria in the system. Additionally, the module should include the transport properties (i.e., diffusivity and viscosity) that are necessary for the computation of flow effects on corrosion. The electrochemical module should predict the surface processes that lead to corrosion as a function of solution chemistry, flow conditions and metal characteristics.

Thus, the objective of this work is to develop a model that

- (1) Utilizes a comprehensive thermodynamic model to compute the activities of species that participate in corrosion processes;
- (2) Includes the partial cathodic and anodic processes that are responsible for general corrosion;
- (3) Incorporates the effect of adsorption of halide ions on the cathodic and anodic processes;
- (4) Represents the active-passive transition and the effect of active ions on passivity;
- (5) Reproduces observed corrosion rates using a reasonable set of physically meaningful parameters and
- (6) Reproduces the effect of pH control and selected inorganic inhibitors on corrosion rates.

## THERMOPHYSICAL MODULE

The starting point for corrosion analysis is the computation of speciation in the investigated system. For this purpose, a realistic model of electrolyte systems is used. This model combines information about standard-state properties of all species of interest with a formulation for the excess Gibbs energy, which accounts for solution nonideality. The model has been described in detail by Zemaitis et al.<sup>4</sup> and Rafal et al.<sup>5</sup> Here, the essential elements of the model are summarized in Appendix A.

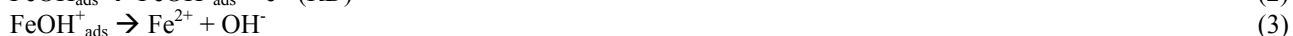
The thermodynamic model is used to predict the concentrations and activities of both ionic and molecular species in multicomponent systems that may contain an aqueous phase, any number of solid phases and, if necessary, a vapor and a nonaqueous liquid phase. The activities of individual species are further used in the electrochemical model. After completing speciation calculations, the module computes the viscosity of the solution and diffusivities of all species using previously developed models.<sup>6,7</sup>

## ELECTROCHEMICAL MODEL

The electrochemical model takes into account reactions on the surface of the metal and transport processes for the species that participate in the reactions. The model focuses on partial cathodic and anodic processes that are expected to be important in systems containing concentrated brines, especially at elevated temperatures. The model takes into account halide adsorption and passivation phenomena, which may be influenced by pH control and inorganic inhibitors. Further, the model combines the partial processes to compute corrosion rates in the framework of the mixed potential theory.

### Electrochemical Reactions in the Absence of Halides

The mechanism of anodic dissolution of iron has been extensively investigated in acidic solutions (cf. a review by Drazic<sup>8</sup>). While several variations of the mechanism have been proposed, the dependence of the dissolution rate on the activity of hydroxide ions is generally accepted. The mechanism proposed by Bockris et al.<sup>9</sup>, i.e.,



predicts that the reaction order with respect to the OH<sup>-</sup> ion is 1. The validity of this prediction has been verified for acidic solutions<sup>9,10</sup>. Additionally, the current density for iron dissolution has been found to depend on the activity of water<sup>11</sup>. The mechanism of Bockris et al.<sup>9</sup> also predicts that the anodic transfer coefficient is equal to 1.5. Thus, the current density for Fe dissolution is given by

$$i_{Fe} = i_{Fe}^0 \exp \left[ \frac{\alpha_{Fe} F (E - E_{Fe}^0)}{RT} \right] \quad (4)$$

where  $i_{Fe}^0$  is the exchange current density,  $\alpha_{Fe} = 1.5$  and  $E^0$  is the reversible potential of Fe dissolution. The exchange current density can be expressed as

$$i_{Fe}^0 = i_{Fe}^* a_{OH} a_{H_2O}^c \quad (5)$$

where  $c$  is a reaction order with respect to the activity of water. According to Smart and Bockris<sup>11</sup>,  $c = 1.6$ . The effect of the activity of water on the current density is very significant for concentrated solutions, for which the activity of water is usually significantly different from one.

Although the reaction order with respect to OH<sup>-</sup> ions is valid for acidic solutions, it has been found that iron dissolution proceeds with little influence of pH for solutions with pH above approximately four<sup>9</sup>. Bockris et al.<sup>9</sup> explained this phenomenon by assuming a certain nonzero reaction order with respect to Fe<sup>2+</sup> and considering the hydrolysis of the Fe<sup>2+</sup> ions that result from the dissolution. Alternatively, the change in the reaction order with respect to OH<sup>-</sup> ions can be reproduced by assuming that the exchange current density is proportional to the surface coverage by OH<sup>-</sup> ions. This assumption is consistent with the reaction mechanism (cf. eq. 1). Thus, eq. (5) can be modified as

$$i_{Fe}^0 = i_{Fe}^* \theta_{OH} a_{H_2O}^c \quad (6)$$

Assuming that  $\theta_{OH}$  follows the Langmuir adsorption model, eq. (6) can be rewritten as

$$i_{Fe}^0 = i_{Fe}^* \frac{a_{OH}}{1 + K_{OH} a_{OH}} a_{H_2O}^c \quad (7)$$

It should be noted that eq. (7) reduces to eq. (5) for low activities of OH<sup>-</sup>, i.e., for acidic solutions. For higher concentrations, the reaction order with respect to OH<sup>-</sup> becomes zero.

The reversible potential is calculated from the Nernst equation<sup>12</sup> and depends on the activity of Fe<sup>2+</sup> ions. As shown by West<sup>48</sup> and Nescic et al.<sup>49</sup>, a relationship exists between the reversible potential and the exchange current density, i.e.,

$$\frac{RT}{\alpha_{Fe} F} \ln \frac{i_{Fe}^0}{i_{Fe}^0} = E_{Fe}^0 - E_{Fe}^0, \quad (8)$$

Eq. (8) makes it possible to compute the exchange current density for any concentration of ferrous ions once it is established for any Fe<sup>2+</sup> concentration. The final expression for the anodic current density in the absence of halide ions is a combination of eqs. (4), (7) and (8).

In general, cathodic processes may be due to the reduction of hydrogen ions or water molecules unless additional reducible species (such as, e.g., oxygen) are present in the solution. In acidic solutions, the reduction of H<sup>+</sup> is the dominant cathodic reaction:



It is generally accepted that the H<sup>+</sup> reduction reaction may proceed under activation or mass transfer control<sup>12</sup>. According to basic electrochemical kinetics<sup>12</sup>, the current density for H<sup>+</sup> reduction can be written as

$$\frac{1}{i_H} = \frac{1}{i_{H,a}} + \frac{1}{i_{H,lim}} \quad (10)$$

where  $i_{H,a}$  and  $i_{H,lim}$  are the activation and limiting current densities, respectively. The activation current density for proton reduction is

$$i_{H,a} = i_H^0 \exp\left[\frac{-\alpha_H F(E - E_H^0)}{RT}\right] \quad (11)$$

where  $\alpha_H = 0.5^9$  and  $E_H^0$  is calculated from the Nernst equation using the previously calculated activities of hydrogen ions and elemental hydrogen. The exchange current density is given by

$$i_H^0 = i_H^* a_H^{0.5} a_{H_2O}^{2.2} \quad (12)$$

In eq. (12), the reaction orders with respect to the activities of  $H^+$  and  $H_2O$  have been obtained from the studies of Bockris et al.<sup>9</sup> and Smart and Bockris<sup>11</sup>.

The limiting current density in eq. (10) results from diffusion-limited transport of protons to the metal surface and can be calculated as

$$i_{H,lim} = k_m F a_H \quad (13)$$

where  $k_m$  is the mass transfer coefficient. The value of  $k_m$  can be calculated if the flow regime, diffusion coefficient of  $H^+$  ions and solution viscosity are known. The formulas for the computation of  $k_m$  are collected in Appendix B.

As the pH of a solution increases, the importance of the proton reduction reaction rapidly decreases. In neutral and alkaline solutions, the predominant reaction is the reduction of water molecules, i.e.,



Unlike the reduction of protons, the water reduction does not exhibit a limiting current density because there are no diffusion limitations for the transport of  $H_2O$  molecules to the surface. Thus, the current density can be expressed as:

$$i_{H_2O} = i_{H_2O}^0 \exp\left[\frac{-\alpha_{H_2O} F(E - E_H^0)}{RT}\right] \quad (15)$$

As in the case of proton reduction,  $\alpha_{H_2O} = 0.5$ . The reversible potential in eq. (15) is the same as in eq. (11) because the reduction of water is thermodynamically equivalent to the reduction of protons. The reaction order with respect to water activity can be assumed to be the same as that for proton reduction. Thus, the exchange current density is given by

$$i_{H_2O}^0 = i_{H_2O}^* a_H^{-0.5} a_{H_2O}^{2.2} \quad (16)$$

For all partial processes, the concentration-independent part of the exchange current density (i.e.,  $i^*$ ) is assumed to be temperature dependent by introducing a non-zero enthalpy of activation, i.e.,

$$i^*(T) = i^*(T_{ref}) \exp\left[-\frac{\Delta H}{R} \left(\frac{1}{T} - \frac{1}{T_{ref}}\right)\right] \quad (17)$$

## Effects of halide adsorption

Adsorption of halide ions on iron and carbon steels has been extensively studied by several investigators.<sup>13-21</sup> In particular, it has been determined that adsorption of halide ions can be quantitatively reproduced using the Frumkin isotherm<sup>19</sup>. This strongly indicates that chemisorption occurs. Halide ions act as good ligands for iron because they exhibit a low electronegativity. Among the halide ions, polarizability increases in the order  $\text{Cl}^- < \text{Br}^- < \text{I}^-$ , which coincides with the increase in the ionic radius. Thus, the tendency for adsorption should also increase in this order. This is in agreement with experimental observations that the adsorption coverage in relatively dilute solutions increases in the order  $\text{Cl}^- < \text{Br}^- < \text{I}^-$ . Thus, at relatively low or moderate halide concentrations, adsorption of halides leads to a reduction in corrosion rates. However, the effect of halides is not limited to blocking the surface through adsorption. The adsorbed halide ions can also interfere with the mechanism of anodic dissolution of iron, which may lead to an increase in the corrosion rate at higher concentrations of halide ions.

For the quantitative representation of the effect of adsorption, we start with the requirement that the rate of adsorption should be equal to the rate of desorption in the stationary state, i.e.,

$$v_{ads,i} = v_{des,i} \quad (18)$$

where the subscript  $i$  denotes any adsorbable species. At the conditions, for which halide adsorption does not interfere with the metal dissolution, the rates can be expressed using the Frumkin isotherm, i.e.,

$$v_{ads,i} = k_{ai} \left( 1 - \sum_j \theta_j \right) a_i \exp \left( -\beta \sum_j A_{ij} \theta_j \right) \quad (19)$$

$$v_{des,i} = k_{di} \left( 1 - \sum_j \theta_j \right) \exp \left( (1 - \beta) \sum_j A_{ij} \theta_j \right) \quad (20)$$

where the transfer coefficient  $\beta$  is commonly assumed to be equal to 0.5,  $a_i$  is the activity of species  $i$  in the bulk solution,  $A_{ij}$  is the Frumkin interaction coefficient and  $k_{a,i}$  and  $k_{d,i}$  are the adsorption and desorption rate constants, respectively.

Combination of the expressions for the adsorption and desorption rates yields the Frumkin isotherm<sup>22</sup> in a version for multicomponent systems, i.e.,

$$\frac{k_{ai}}{k_{di}} a_i = \frac{\theta_i}{1 - \sum_j \theta_j} \exp \left( \sum_j A_{ij} \theta_j \right) \quad (21)$$

In eq. (21), the  $k_{a,i}$  and  $k_{d,i}$  constants are not independently measurable and only their ratio can be established.

Eq. (21) is valid only when adsorption is not significantly influenced by metal dissolution. To include the effect of dissolution, Heusler and Cartledge<sup>14</sup> proposed an additional process in which a metal atom from an uncovered  $(1 - \Sigma\theta)$  area reacts with a hydroxyl ion and an adsorbed halide ion from the covered area  $\theta_i$  to dissolve as ferrous ion. The adsorbed halide was postulated to leave the surface during the reaction, thus contributing to the desorption process. This mechanism was confirmed by matching calculated and measured polarization curves<sup>14</sup>. To include the effect of dissolution-related desorption, eq. (20) can be rewritten by adding an additional term, i.e.,

$$v_{des,i} = k_{di} \left( 1 - \sum_j \theta_j \right) \exp \left( (1 - \beta) \sum_j A_{ij} \theta_j \right) + i_{des,i} \quad (22)$$

where the desorption current  $i_{des,i}$  is given by

$$i_{des,i} = k_{ri} \theta_i \left( 1 - \sum_j \theta_j \right) a_{OH} \exp \left( \frac{2\beta FE}{RT} \right) \quad (23)$$

In eq. (23), the desorption current is potential-dependent because it involves the dissolution of the metal. Thus, eq. (23) can be combined with eqs. (19) and (22) to form a system of  $n$  nonlinear equations for a solution with  $n$  adsorbable species. This system can be solved numerically for the coverage fractions  $\theta_i$  of each adsorbed species. Because of the potential dependence, the model predicts that the adsorption coverage rapidly decreases above a certain potential range, which depends primarily on the activity of halide and hydroxide ions.

The three reaction rate constants  $k_{ai}$ ,  $k_{di}$  and  $k_{ri}$  are not independent and only the ratios  $k_{di}/k_{ai}$  and  $k_{ri}/k_{ai}$  can be determined. Thus, the adsorption model described above is characterized by  $k_{di}/k_{ai}$ ,  $k_{ri}/k_{ai}$  and  $A_{ij}$  as parameters. These parameters have been obtained by analyzing experimental polarization and, secondarily, corrosion rate data for varying concentrations of halide ions.<sup>13,16,17,19-21</sup>

### Halide-accelerated dissolution

In concentrated solutions, adsorbed halide ions may accelerate the dissolution of iron or carbon steel. A number of reaction mechanisms has been proposed to explain this phenomenon. In particular, Chin and Nobe<sup>16</sup> and Kuo and Nobe<sup>17</sup> developed a mechanism that postulates a reaction route that is parallel to eqs. (1-3). An essentially identical mechanism has also been proposed by Drazic and Drazic<sup>20</sup>. According to this mechanism, a halide-containing surface complex is responsible for the dissolution. Thus, eq. (1) is followed by the following parallel route:



The mechanism (24-26) results in a dissolution current density that depends on the activities of both halide and hydroxide ions, i.e.,

$$i_{\text{Fe},\text{X}} = i_{\text{Fe},\text{X}}^* a_{\text{X}^-}^s a_{\text{OH}^-}^t \exp\left(\frac{F(E - E_{\text{Fe}}^0)}{RT}\right) \quad (27)$$

For chloride systems, Kuo and Nobe<sup>17</sup> found that  $s = 0.4$  and  $t = 0.6$  when concentrations are used instead of activities. For bromide systems, the reaction orders determined in this study are  $s = 1$  and  $t = 3$ . Since the mechanism described by eqs. (24-26) is assumed to be parallel to the mechanism under halide-free conditions, the total current density of anodic dissolution can be assumed to be a sum of the contributions of two mechanisms. Additionally, the desorption current density (eq. 23) contributes to the total current, although it becomes important only at relatively high potentials and its numerical significance is usually limited. Thus, the expression for the total current becomes:

$$i_{\text{Fe}}' = i_{\text{Fe}} + i_{\text{Fe},\text{X}} + \sum_j i_{\text{des},j} \quad (28)$$

### Modeling the active-passive transition

Corrosion control strategies for adsorption refrigeration systems rely on influencing passivity at high temperatures using inhibitors. Thus, it is necessary to introduce the active-passive transition into the expression for the anodic current density. For this purpose, a convenient method has been developed by Ebersbach et al.<sup>23</sup> According to the approach of Ebersbach et al., the current that leads to the formation of a passive layer is considered separately from the current that leads to active dissolution. At any instant, a certain fraction of the surface  $\theta_p$  is assumed to be covered by the passive layer. The change of the passive layer coverage fraction with time can be expressed as

$$\left(\frac{\partial \theta_p}{\partial t}\right)_{E,a_i} = ci_2(1 - \theta_p) - K\theta_p \quad (29)$$

where  $i_2$  is the current density that contributes to the formation of a passive layer. The second term on the right-hand side of eq. (29) represents the rate of dissolution of the passive layer, which is proportional to the coverage fraction. The parameters  $c$  and  $K$  are proportionality constants. The total current density is expressed as

$$i_{Fe,TOT} = (i_{Fe}' + i_2)(1 - \theta_p) \quad (30)$$

where  $i_{Fe}'$  is the current density for active dissolution of iron. Eq. (29) can be solved with respect to  $\theta_p$  and the result can be substituted into eq. (30). In the stationary state ( $t \rightarrow \infty$ ), the total anodic current becomes

$$i_{Fe,TOT} = \frac{i_{Fe}' + i_2}{1 + \frac{ci_2}{K}} = \frac{i_{Fe}' + i_2}{1 + \frac{i_2}{i_p}} \quad (31)$$

In eq. (31), the ratio  $c/K$  constitutes the passive current density. The current density  $i_2$  can be represented by the usual expression for processes under activation control, i.e.,

$$i_2 = i_2^0 \exp\left(\frac{\alpha_2 F(E - E_F)}{RT}\right) \quad (32)$$

Thus, in addition to the passive current density, the model of the active-passive transition is characterized by two parameters, i.e.,  $i_2^0$  and  $\alpha_2$ . These parameters are determined based on observable characteristics of the active-passive transition such as the Flade potential and the critical current density<sup>12,24</sup>.

### Effect of Solution Chemistry on Passivation

In the absence of active ions, the passive current density depends primarily on the pH of the solution<sup>12</sup>. Halide ions cause the breakdown of passive films, which manifests itself in an increase in the passive current in addition to the onset of localized corrosion<sup>25</sup>. On the other hand, corrosion inhibitors such as molybdates or chromates may repair passive films, thus reducing the passive current density. In this study, we are not concerned with localized corrosion and examine only the effect of halide ions on the magnitude of the passive current density.

As shown by Vetter<sup>12</sup>, the pH dependence of the corrosion current density in the passive state is determined by a reaction between  $O^{2-}$  ions in the passive oxide layer and protons from the solution. In acidic solution, this dissolution reaction can be written as



where the symbol “ $\equiv$ ” denotes the solid substrate and the formula  $FeOOH$  approximates the hydrated oxide in the passive layer, although different stoichiometries are also plausible. Reaction (33) leads to a linear dependence of the passive current density on pH, which is in agreement with experimental data in acidic solutions<sup>26</sup>. For neutral and alkaline solutions, reaction (33) can be modified as



Reactions (33) and (34) lead to an expression for the passive current density, i.e.,

$$i_p = k_H a_{H^+}^b + k_{H_2O} a_{H_2O} \quad (35)$$

Eq. (35) predicts a linear pH dependence of  $i_p$  in acidic solutions and a pH-independent value for nearly neutral or alkaline solutions. This behavior agrees with the results of Vetter<sup>12,26</sup> and Sato et al.<sup>24</sup>

To analyze the effect of active ions on the passive current density, we consider surface reactions between the passive oxide layer and solution ions<sup>27</sup>, i.e.,



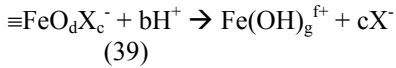
In eq. (36), the stoichiometry is usually difficult to define because of the dynamic nature of the system and may be, in general, fractional. It is reasonable to assume that eq. (36) is in quasi-equilibrium<sup>27</sup>. Therefore, it may be characterized by an equilibrium constant, i.e.,

$$K_i = \frac{N_i a_{\text{OH}^-}^{e_i}}{(N_0 - \sum_k N_k) a_{\text{X}_i}^{c_i}} \quad (37)$$

where the subscript  $i$  pertains to the  $i$ -th active ion,  $N_i$  is the number of sites per surface unit that are occupied by complexes containing the  $i$ -th active ion and  $N_0$  is the total number of sites per surface area. Eq. (37) represents a system of equations that may represent surface reaction involving any number of active species. This system may be solved with respect to  $N_i$ , i.e.,

$$N_i = \frac{N_0 K_i \frac{a_{\text{X}_i}^{c_i}}{a_{\text{OH}^-}^{e_i}}}{1 + \sum_k K_k \frac{a_{\text{X}_k}^{c_k}}{a_{\text{OH}^-}^{e_i}}} \quad (38)$$

The surface reaction (36) is followed by a dissolution reaction. The surface species that forms as a result of reaction (36) may undergo a dissolution reaction that is analogous to reaction (33), i.e.,



The dissolution rate for the sites occupied by complexes with active ions is given by

$$i_{p,i} = k_i N_i a_{\text{H}^+}^b \quad (40)$$

whereas the dissolution rate for the free sites is

$$i_{p,0} = k_H \left( N_0 - \sum_k N_k \right) a_{\text{H}^+}^b \quad (41)$$

The total current density in the passive state is the sum of eqs. (40) and (41), i.e.,

$$i_p = i_{p,0} + \sum_k i_{p,k} \quad (42)$$

Analogous expressions can be written for the dissolution in neutral and alkaline solutions. Assuming that the surface reactions (eq. 36) are characterized by the same parameters over the whole pH range, the total passive current density can be expressed as

$$i_p = \left( k_H a_{\text{H}^+}^b + k_{\text{H}_2\text{O}} a_{\text{H}_2\text{O}} \right) \frac{1 + \sum_i l_i \frac{a_{\text{X}_i}^{c_i}}{a_{\text{OH}^-}^{e_i}}}{1 + \sum_i K_i \frac{a_{\text{X}_i}^{c_i}}{a_{\text{OH}^-}^{e_i}}} \quad (43)$$



where  $l_i$  is a composite parameter that contains both the forward dissolution rate constant ( $k_i$ ) and the quasi-equilibrium constant  $K_i$ . In eq. (43), the  $k_H$  and  $k_{H_2O}$  parameters are determined using data for passive film dissolution in the absence of active ions.<sup>12,24,26</sup> Halide ions are characterized by both the  $l_i$  and  $K_i$  parameters because surface reaction is followed by dissolution. Inhibitor ions, such as  $MoO_4^{2-}$ , are characterized by only the  $K_i$  parameters and the value of  $l_i$  is equal to zero. Thus, according to the model, inhibitor ions are envisaged to form surface complexes that block the reaction sites on the surface of the passive layer. In this case, the surface reaction is not followed by accelerated dissolution. Thus, the presence of inhibitor ions limits the current density. In this way, the model takes into account the ions that promote the dissolution of the passive film ( $K_i \neq 0$  and  $l_i \neq 0$ ) and those that inhibit the dissolution ( $K_i \neq 0$  and  $l_i = 0$ ).

## Implementation of the model

The parameters of the electrochemical model have been determined by utilizing a large number of experimental polarization and corrosion rate data. To ensure the validity of the model under a substantial range of conditions, these data were not limited to corrosion in LiBr-based systems. In particular, the parameters for the proton reduction, water reduction and iron oxidation processes were determined from data on the corrosion of iron and mild steel in various mineral acids, bases and saline solutions.<sup>28,29</sup> Corrosion data for LiBr+H<sub>2</sub>O were utilized only for establishing the parameters of the processes that are specific to LiBr corrosion (e.g., the bromide-assisted anodic dissolution).

The model described above has been implemented in a program for the prediction and analysis of corrosion rates. As input, the program accepts the composition of corrosive medium, temperature and pressure. Then, thermodynamic calculations are performed to compute the speciation of the system and predict the stable phases. Depending on the conditions, the system may be made up of an aqueous phase that includes electrolyte components, a gas phase and any number of solid phases. The thermodynamic calculations make it possible to obtain the concentrations and activities of individual species, which are used further as input for the electrochemical model. Additionally, the program returns the diffusivities of individual species and the viscosity of the aqueous phase.

To execute the electrochemical model, the program requires flow conditions as additional input. Currently, the flow conditions are limited to single-phase flow. In addition to static conditions, pipe flow, rotating disk or rotating cylinder conditions can be selected. Then, the program computes the current density – potential relationships for individual cathodic and anodic processes. Further, the individual processes are combined into a total predicted polarization curve. The corrosion potential is calculated by applying the mixed-potential theory, i.e.,

$$\sum i_{c,i} = \sum i_{a,j} \quad (44)$$

where  $i_{c,i}$  and  $i_{a,j}$  denote the  $i$ -th cathodic and  $j$ -th anodic process. Once the corrosion potential is obtained by solving eq. (44), the corrosion current density is also computed.

After performing the calculations, the program displays the predicted corrosion rates and current density – potential relationships. Also, the program makes it possible to perform parametric studies in which the effect of various variables (e.g., temperature, pressure, concentration of selected components, flow velocity, etc.) on corrosion rate can be analyzed.

## RESULTS AND DISCUSSION

First, the thermodynamic model has been verified by using experimental vapor pressure and solubility data for lithium bromide-based systems. Figure 1 shows the results of vapor pressure calculations for the LiBr+H<sub>2</sub>O solution in wide concentration ranges at temperatures up to 573 K. Very good agreement with experimental data from various sources has been obtained. Similarly, Figure 2 shows a solubility diagram for LiBr+H<sub>2</sub>O, which is characterized by the presence of four separate hydrates as solid phases. The model represents the data within experimental uncertainty. Results of thermodynamic calculations for more complex absorption cooling systems have been reported in a separate study<sup>30</sup>. The agreement with experimental vapor pressure and solubility data indicates that the model correctly reproduces the activities of solution species. Thus, the activities can be used with confidence in the electrochemical model.

After validating the thermodynamic module, the electrochemical model has been applied first to systems that clearly show the effect of halide adsorption on corrosion rates. To verify the effect of adsorption, it is convenient to analyze

corrosion rates with respect to changing concentrations of halide ions. Such analysis is shown in Figure 3 for a mixture containing  $\text{H}_2\text{SO}_4$ ,  $\text{Na}_2\text{SO}_4$  and increasing amounts of KCl and another mixture containing HCl and increasing amounts of KCl. Since the halide concentrations shown in Figure 3 are moderate (up to 3 M), adsorption results primarily in a reduction of corrosion rates. The calculated results are in good agreement with the data of Schwabe and Voigt<sup>13</sup>. It is noteworthy that the decrease in corrosion rates is observed primarily for dilute solutions and the rates appear to stabilize at higher concentrations. This is in agreement with the results of Jesionek and Szklarska-Smialowska<sup>19</sup>, who have shown that substantial surface coverages are obtained for relatively dilute halide solutions.

In addition to halide ion concentrations, pH is an important independent variable. Therefore, calculations have been performed for the corrosion of iron in systems with a fixed amount of halide ions and varying pH. The results are shown in Figure 4 for 1 M solutions of HBr and KBr with varying pH<sup>25</sup>. As shown in Figure 4, the pH effect is reproduced with good accuracy.

As the activity of halide ions increases to high values, the corrosion rate increases because of halide-assisted dissolution (cf. eq. 27). For LiBr solutions, this is observed for concentrations exceeding ca. 3-4 m. This is illustrated in Figure 5 for the LiBr- $\text{H}_2\text{O}$  system at 25 C. The increase in corrosion rate with increasing Br concentrations in near-neutral solutions is relatively slow and the rate levels off at very high concentrations. As shown in Figure 5, the model reproduces the data of Guñón et al.<sup>2</sup> with very good accuracy.

At elevated temperatures, which are of primary interest for absorption cooling cycles, the experimental corrosion rates are inherently much more uncertain. This is illustrated in Figure 6 for LiBr+ $\text{H}_2\text{O}$  at temperatures ranging from 100 to 160 C and three concentrations. The data show significant scattering, especially at the highest concentration. As with corrosion rates at low temperatures, a relatively moderate increase in corrosivity is observed with concentration. The model is consistent with the data and the computed corrosion rates are within the limits of experimental uncertainty. The model predicts that the corrosion rates increase with temperature, but the slope of the rate versus temperature curves is relatively small. It should be noted that the results shown in Figure 6 have been obtained on the assumption that the solution is static, which is a reasonable assumption for a solution in an unstirred autoclave. Under static conditions in the near-neutral LiBr solutions, the reduction of protons is unimportant and the only significant cathodic reaction is the reduction of water molecules. In somewhat agitated solutions, the hydrogen reduction reaction could make an additional contribution to the corrosion process because hydrogen reduction is mass-transfer-limited. Thus, some agitation could explain the corrosion rates that lie above the calculated values in Figure 6.

The primary practical problem in the control of corrosion in absorption cooling cycles is the selection of inhibitors. Because of high temperatures that may cause the decomposition of organic molecules, inorganic inhibitors are of primary significance. The inhibition of corrosion in bromide systems involves both pH control and the application of inhibitors such as molybdates or chromates. Therefore, the model has been applied to study their effect on corrosion rates.

First, the effect of increasing the pH has been analyzed. As shown by eq. (43), the passive current density is a function of activities of ions that promote the dissolution of passive films, such as the bromide ions. At the same time, the passive current density depends on the activity of hydroxide ions, which play a role in the dissolution reaction according to eq. (43). In general, an increase in  $\text{OH}^-$  ion concentration reduces the passive current density. However, the interplay between the  $\text{Br}^-$  and  $\text{OH}^-$  ions may lead to a complex behavior of corrosion rates.

Figure 7 shows the predicted current density - potential relationship for carbon steel at 160 C in a static LiBr solution without any pH-adjusting agents. The corrosion rate is determined by two partial processes, i.e., the oxidation of iron and reduction of water. The system is predicted to be in the active corrosion range. The change in the slope of the anodic curve at potentials around -0.4 is a result of the potential dependence of the adsorption process. The bromide ions become desorbed in the potential range where the anodic curve is nearly flat. Although no polarization data are available to confirm this behavior for LiBr brines at high temperatures, this phenomenon is well known for chloride and iodide solutions at room temperature<sup>14,16</sup>. The range of a significantly reduced slope of potential versus the current density was experimentally identified by Heusler and Cartledge<sup>14</sup> and called the unpolarizability range.

Figure 8 shows the change in the predicted polarization behavior when 0.1m LiOH is added to the same system. This causes a shift into the passive state as shown by the nearly-vertical portion of the anodic curve. The mixed potential is shifted to a significantly higher value and the corrosion current density is reduced. The shape of the cathodic curve in Figure 8 is a result of the potential dependence of adsorption. This behavior remains hypothetical because no experimental polarization data are available to verify it.

In contrast to the lack of polarization data, corrosion rate data are available from exposure experiments<sup>3</sup> and make it possible to verify the predictions of the model. Figures 9 and 10 show the predicted corrosion rate as a function of LiOH molality for carbon steel at 160 and 120 C, respectively. In the case of LiBr solutions with relatively low and moderate concentrations (i.e., 5, 7.5 and 10 m), the corrosion rate is significantly reduced by the presence of LiOH. The concentration of LiOH that is necessary for the reduction of corrosion rates depends on the LiBr concentration and is predicted to vary from approximately 0.02 to 0.08 m. It is noteworthy that the corrosion rate for moderately concentrated LiBr solutions reaches a minimum at LiOH concentrations between 0.05 and 0.08m and slowly increases as the LiOH molality rises. This is a result of the complicated dependence of the passive current density on the activities of bromide and hydroxide ions (cf. eq. 43). The model predictions are fully consistent with experimental data of Tanno et al.<sup>31</sup> Although the data show a significant degree of scattering (cf. Figs. 9 and 10), no systematic deviations are observed between the calculated results and experimental data. Also, a similar trend with a shallow minimum in the corrosion rate as a function of LiOH concentration was determined for somewhat different conditions by Dockus et al.<sup>32</sup>

It is noteworthy that the effect of LiOH on corrosion rates becomes much less significant when the LiBr concentration is high (e.g., 23 m in Figure 9). In this case, the model predicts only a small dip in corrosion rate as a function of LiOH molality. The experimental data are consistent with the calculated results despite substantial scattering. In this case, the activity of bromide ions is so high that it practically overwhelms the effect of hydroxide ions.

The above results show that pH control is effective for reducing corrosion rates when the concentration of LiBr is not excessively high. In such cases, corrosion rates well below 1 mpy are obtained. For very concentrated LiBr solutions, it is necessary to use additional inhibitors to reduce the rate to an acceptable level. In this study, we analyze the inhibiting effect of lithium molybdate.

Molybdates are generally known to reduce the passive current density<sup>33</sup>. Under typical conditions at low or moderate temperatures, it is necessary to use molybdates in conjunction with selected oxidizing agents (e.g., nitrites) to increase the potential and, in this way, shift the mixed potential to the passive region<sup>34</sup>. However, the use of additional oxidizing agents does not seem to be necessary at elevated temperatures that are of interest for absorption cooling cycles. In this case, a reduction in the passive current density may be sufficient to reduce corrosion rates. Thus, molybdates can be expected to reinforce the effect of hydroxide ions, which are capable of reducing corrosion for LiBr solutions up to moderate concentrations.

Figure 11 shows the effect of molybdate ions on the corrosion rates in solutions containing 0.1 m LiOH and various concentrations of LiBr. In the case of solutions with low and moderate concentrations of LiBr (i.e., 2 and 10 m), the corrosion rates are already low in the absence of molybdate ions and the addition of  $\text{Li}_2\text{MoO}_4$  results in only a marginal reduction of corrosivity. However, the effect of  $\text{Li}_2\text{MoO}_4$  is very significant for the highest concentrations of LiBr (i.e., 23m). In this case, a small amount of molybdate ions (i.e., approximately 0.002 m) reduces the corrosion rate to a low value. The results of computations agree very well with the experimental data of Tanno et al.<sup>31</sup> Thus, the synergistic effect of hydroxide and molybdate ions is accurately represented by the expression for the dependence of passive current density on concentrations of active ions (eq. 43).

## CONCLUSIONS

A comprehensive model has been developed for simulating the rates of general corrosion of carbon steels in lithium bromide-based working fluids, which are used in absorption refrigeration cycles. The model consists of a thermophysical module that provides comprehensive speciation calculations and an electrochemical module that predicts the partial reduction and oxidation processes on the surface of the metal. The model has been extensively validated using both thermodynamic and corrosion rate data. Good agreement with experimental data has been obtained. Although the predicted current density - potential relationships cannot be verified due to a lack of polarization data for LiBr solutions at high temperatures, the predicted corrosion rates are in quantitative agreement with rates obtained from coupon experiments. It is noteworthy that the model accurately represents the effect of pH control and molybdate inhibitors on corrosion rates. The model can be extended to include other inhibitors and, thus, it can serve as a prediction tool for designing corrosion inhibition strategies.

The model has been incorporated into a program that can be used to study the effect of conditions such as temperature, pressure, pH, solution composition or flow velocity on corrosion rates. The program has been integrated with the previously developed components of the OLI software<sup>35</sup>, which make it possible, among various capabilities, to simulate the thermodynamic behavior of aqueous solutions.

## ACKNOWLEDGEMENT

The authors gratefully acknowledge the financial support of the Gas Research Institute under the contract 5096-260-3596 and the technical guidance provided by Dr. Kevin Krist. The authors greatly benefited from discussions with Dr. Stephen Kujak of the Trane Company.

## REFERENCES

1. K. E. Herold, R. Radermacher, S. A. Klein, Absorption Chillers and Heat Pumps: CRC Press, Boca Raton, FL (1996).
2. J. L. Guñon, J. Garcia-Anton, V. Perez-Herranz, G. Lacoste, Corrosion, v. 50, p. 240-246 (1994).
3. K. Tanno, M. Itoh, T. Takahashi, H. Yashiro, N. Kumagai, Corrosion Sci., v. 34, p. 1441-1451 (1993).
4. J.F. Zemaitis, Jr., D. M. Clark, M. Rafal, N. C. Scrivner, Handbook of aqueous electrolyte thermodynamics: AIChE, New York, NY, 852 p. (1986).
5. M. Rafal, J. W. Berthold, N. C. Scrivner, S. L. Grise, Models for electrolyte solutions, in S. I. Sandler, ed., Models for Thermodynamic and Phase Equilibria Calculations: M. Dekker, New York, NY, p. 601-670 (1995).
6. M. M. Lencka, A. Anderko, S.J. Sanders, R. D. Young, Int. J. Thermophysics, v. 19, p. 367-378 (1998).
7. A. Anderko, M. M. Lencka, Ind. Eng. Chem. Res., v. 37, p. 2878-2888 (1998).
8. D. M. Drazic, Iron and Its Electrochemistry in an Active State, in B. E. Conway, J. O'M. Bockris, R. E. White, eds., Modern Aspects of Electrochemistry, No. 19 : Plenum Press, New York, NY, p. 69-192 (1989).
9. J. O'M. Bockris, D. Drazic, A. R. Despic, Electrochim. Acta, v. 4, p. 325-361 (1961).
10. E. J. Kelly, J. Electrochem. Soc., v. 112, p. 124-131 (1965).
11. N. G. Smart and J. O'M. Bockris, Corrosion, v. 48, p. 277-280 (1992).
12. K. J. Vetter, Electrochemical Kinetics: Academic Press, New York, NY (1967).
13. K. Schwabe, C. Voigt, Electrochim. Acta, v. 14, p. 853-869 (1969).
14. K. E. Heusler, G. H. Cartledge, J. Electrochem. Soc., v. 108, p. 732-740 (1961).
15. K. Nobe, R. F. Tobias, Corrosion, v. 20, p. 263t-266t (1964).
16. R. J. Chin, K. Nobe, J. Electrochem. Soc., v. 119, p. 1457-1461 (1972).
17. H. C. Kuo, K. Nobe, J. Electrochem. Soc., v. 125, p. 853-860 (1978).
18. E. McCafferty, N. Hackerman, J. Electrochem. Soc., v. 119, p. 999-1009 (1972).
19. M. Jesionek, Z. Szklarska-Smialowska, Corrosion Sci., v. 23, p. 183-187 (1983).
20. V. J. Drazic, D. M. Drazic, J. Serb. Chem. Soc., v. 57, p. 917-926 (1992).
21. Lj. Vracar, D. M. Drazic, J. Electroanal. Chem., v. 339, p. 269-279 (1992).
22. E. Gileadi, ed., Electrosorption: Plenum Press, New York, NY (1967).
23. U. Ebersbach, K. Schwabe, K. Ritter, Electrochim. Acta, v. 12, p. 927-938 (1967).
24. N. Sato, T. Noda, K. Kudo, Electrochim. Acta, v. 19, p. 471-475 (1974).
25. L. P. Mack, K. Nobe, Corrosion, v. 40, p. 215-219 (1984).
26. K. J. Vetter, Z. Elektrochem., v. 59, p. 67 (1955).
27. M. A. Blesa, P. J. Morando, A. E. Regazzoni, Chemical Dissolution of Metal Oxides: CRC Press, Boca Raton, FL (1994).
28. B. D. Craig, D. S. Anderson, eds., Handbook of Corrosion Data: ASM International, Materials Park, OH (1995).
29. P. B. Mathur, T. Vasudevan, Corrosion, v. 38, p. 171-178 (1982).
30. A. Anderko, M. M. Lencka, Speciation Modeling of Advanced LiBr Absorption Cooling Fluids, Topical Technical Report No. GRI-97/0027: Gas Research Institute, Chicago, IL (1997).
31. K. Tanno, M. Itoh, H. Sekiya, H. Yashiro, N. Kumagai, Corrosion Sci., v. 34, p. 1453-1461 (1993).
32. K. F. Dockus, R. H. Krueger, W. F. Rush, ASHRAE J., no. 12, p. 67 (1962).
33. M. A. Stranick, Corrosion, v. 40, p. 296-302 (1984).
34. M. S. Vukasovich, in A. Raman, P. Labine, Reviews on Corrosion Science and Technology, p. II-12-1: NACE International, Houston, TX (1993).
35. OLI Software Manual: OLI Systems Inc., Morris Plains, NJ (1998).
36. H. C. Helgeson, D. H. Kirkham, G. C. Flowers, Am. J. Sci., v. 281, p. 1249-1516 (1981).
37. J. C. Tanger, H. C. Helgeson, Am. J. Sci., v. 288, p. 19-98 (1988).
38. E. L. Shock, H. C. Helgeson, Geochim. Cosmochim. Acta, v. 52, p. 2009-2036 (1988).
39. E. L. Shock, H. C. Helgeson, Geochim. Cosmochim. Acta, v. 54, p. 915-943 (1990).
40. D. A. Sverjensky, Reviews in Mineralogy, v. 17, p. 177-209 (1987).

41. L. A. Bromley, *AIChE J.*, v. 19, p. 313-320 (1973).
42. K. S. Pitzer, *J. Phys. Chem.*, v. 77, p. 268-277 (1973).
43. G. Soave, *Chem. Eng. Sci.*, v. 27, p. 1197-1203 (1972).
44. H. P. Meissner, *in* S.A. Newman, ed., *Thermodynamics of Aqueous Systems with Industrial Applications: Am. Chem. Soc. Symp. Ser.*, v. 133, p. 495-511 (1980).
45. V.G. Levich, *Physicochemical Hydrodynamics: Prentice-Hall, Englewood Cliffs, NJ*, 700 p. (1962).
46. F. P. Berger, K.-F. F. L. Hau, *Int. J. Heat Mass Trans.*, v. 20, p. 1185-1194 (1977).
47. M. Eisenberg, C. W. Tobias, C. R. Wilke, *J. Electrochem. Soc.*, v. 101, p. 306-319 (1954).
48. J. M. West, *Electrodeposition and Corrosion Processes: Van Nostrand, New York, NY* (1964).
49. S. Nescic, J. Postlethwaite, S. Olsen, *Corrosion*, v. 52, p. 280-294 (1996).
50. M. K. Fedorov, N. A. Antonov, S. N. Lvov, *Russ. J. Appl. Chem.*, v. 49, p. 1263-1268 (1976).
51. D.A. Boryta, *J. Chem. Eng. Data*, v. 20, p. 316-319 (1973).
52. K. Murakami, H. Sato, K. Watanabe, *Int. J. Thermophysics*, v. 16, p. 811-820 (1995).
53. T. Uemura, S. Hasaba, S, *Tech. Rep. Kansai Univ.*, v. 6, p. 31-55 (1964).
54. W. Pennington, *Refriger. Eng.* p. 57-61 (1955).
55. J. J. Kessiss, *Bull. Soc. Chim.*, 48-52 (1965).
56. D. A. Boryta, *J. Chem. Eng. Data*, v. 15, p. 142-144 (1970).
57. C. O. Adegoke, *Int. J. Refriger. (Rev. Int. Froid)*, v. 16, p. 45-48 (1993).

## APPENDIX A: THERMODYNAMIC FRAMEWORK

In a multicomponent system, the partial molal Gibbs energy of the *i*-th species is related to the molality ( $m_i$ ) by

$$\bar{G}_i = \bar{G}_i^0 + RT \ln m_i \gamma_i \quad (\text{A-1})$$

where  $\bar{G}_i^0$  is the standard-state partial Gibbs energy and  $\gamma_i$  is the activity coefficient. Thus, the thermodynamic properties of the system can be calculated if the standard-state Gibbs energies are available for all species as functions of temperature and pressure (i.e.,  $\bar{G}_i^0(T, P)$ ) and the activity coefficients are known as functions of the composition vector  $\mathbf{m}$  and temperature (i.e.,  $\gamma_i(\mathbf{m}, T)$ ). From basic thermodynamics, the standard-state Gibbs energy of formation  $\bar{G}_i^0(T, P)$  can be calculated as a function of temperature and pressure if the following data are available:

- (1) Gibbs energy of formation at a reference temperature and pressure (usually,  $T_r = 298.15$  K and  $P_r = 1$  bar);
- (2) Enthalpy of formation at  $T_r$  and  $P_r$ ;
- (3) Entropy at  $T_r$  and  $P_r$ ;
- (4) Heat capacity as a function of temperature and pressure and
- (5) Volume as a function of temperature and pressure

The key to representing the standard-state properties over substantial temperature and pressure ranges is the accurate knowledge of the heat capacity and volume. For this purpose, the Helgeson-Kirkham-Flowers-Tanger<sup>36,37</sup> equation of state is used. This equation accurately represents the standard-state thermodynamic functions for aqueous, ionic or neutral, species as functions of both temperature and pressure. In its revised form<sup>37</sup>, the HKFT equation is capable of reproducing the standard-state properties up to 1000 °C and 5 kbar.

The HKFT equation is based on the solvation theory and expresses the standard-state thermodynamic functions as sums of structural and solvation contributions, the latter being dependent on the properties of the solvent (i.e., water). The standard partial molal volume ( $\bar{V}^0$ ) and heat capacity ( $\bar{C}_p^0$ ) are given by:

$$\bar{V}_0 = a_1 + \frac{a_2}{\Psi + P} + \left( a_3 + \frac{a_4}{\Psi + P} \right) \left( \frac{1}{T - \Theta} \right) - \omega Q + \left( \frac{1}{\varepsilon} - 1 \right) \left( \frac{\partial \omega}{\partial P} \right)_T \quad (\text{A-2})$$

$$\bar{C}_p^0 = c_1 + \frac{c_2}{(T - \Theta)^2} - \left( \frac{2T}{(T - \Theta)^3} \right) \left( a_3(P - P_r) + a_4 \ln \frac{\Psi + P}{\Psi + P_r} \right) + \omega TX + 2TY \left( \frac{\partial \omega}{\partial T} \right)_P - T \left( \frac{1}{\varepsilon} - 1 \right) \left( \frac{\partial^2 \omega}{\partial T^2} \right)_P \quad (\text{A-3})$$

where  $a_1$ ,  $a_2$ ,  $a_3$ ,  $a_4$ ,  $c_1$  and  $c_2$  represent species-dependent nonsolvation parameters,  $T_r$  is the reference temperature of 298.15 K,  $P_r$  is the reference pressure of 1 bar,  $\Psi$  and  $\Theta$  refer to solvent parameters equal to 2600 bars and 228 K, respectively,  $Q$ ,  $X$ , and  $Y$  denote the Born functions given by

$$Q = \frac{1}{\varepsilon} \left( \frac{\partial \ln \varepsilon}{\partial P} \right)_T \quad (\text{A-4})$$

$$X = \frac{1}{\varepsilon} \left[ \left( \frac{\partial^2 \ln \varepsilon}{\partial T^2} \right)_P - \left( \frac{\partial \ln \varepsilon}{\partial T} \right)_P^2 \right] \quad (\text{A-5})$$

$$Y = \frac{1}{\varepsilon} \left( \frac{\partial \ln \varepsilon}{\partial T} \right)_P \quad (\text{A-6})$$

where  $\varepsilon$  is the dielectric constant of water and  $\omega$  stands for the Born coefficient, which is defined for the  $j$ -th aqueous species by

$$\omega_j \equiv \omega_j^{abs} - Z_j \omega_{H^+}^{abs} \quad (\text{A-7})$$

In equation (A-7),  $Z_j$  is the charge on the  $j$ -th aqueous species,  $\omega_{H^+}^{abs}$  refers to the absolute Born coefficient of the hydrogen ion and  $\omega_j^{abs}$  designates the absolute Born coefficient of the  $j$ -th species given by

$$\omega_j^{abs} = \frac{N^0 e^2 Z_j^2}{2r_{e,j}} \quad (\text{A-8})$$

where  $N^0$  is the Avogadro number,  $e$  is the electron charge and  $r_{e,j}$  denotes the effective electrostatic radius of the  $j$ -th species, which is related to the crystallographic radius  $r_{x,j}$  by

$$r_{e,j} = r_{x,j} + |z_j| (k_z + g) \quad (\text{A-9})$$

where  $k_z$  represents a charge-dependent constant equal to 0.0 for anions and 0.94 for cations and  $g$  denotes a generalized function of temperature and density. Thus, the HKF equation expresses the heat capacity and volume as functions of pure water properties and seven empirical parameters, which have been tabulated for large numbers of ions, complexes and neutral, both inorganic and organic, molecules. The remaining thermodynamic properties are obtained by thermodynamic integration using the values of the Gibbs energy, enthalpy and entropy at reference temperature and pressure as integration constants.

If the HKF equation parameters are not available from the regression of experimental data, they can be estimated. For this purpose, Shock and Helgeson<sup>38,39</sup> presented correlations for most solution species except for complexes. Sverjensky<sup>40</sup> developed an estimation method for several classes of complexes. In addition to the HKF equation parameters, these methods make it possible to predict the reference-state enthalpy and entropy if the reference-state Gibbs energy is known. These and other estimation techniques have been reviewed in detail by Rafal et al.<sup>5</sup>

The activity coefficient model used for representing the solution nonideality is an extended form of an expression developed by Bromley.<sup>41</sup> The Bromley equation is a combination of the Debye-Hückel term for long-range electrostatic

interactions and a semi-empirical expression for short-range interactions between cations and anions. In a multicomponent system, the activity coefficient of an ion  $i$  is given by

$$\log \gamma_i = \frac{-Az_i^2 I^{1/2}}{1+I^{1/2}} + \sum_j^{NO} \left[ \frac{|z_i| + |z_j|}{2} \right]^2 \left[ \frac{(0.06 + 0.6B_{ij})|z_i z_j|}{\left(1 + \frac{1.5}{|z_i z_j|} I\right)^2} + B_{ij} + C_{ij} I + D_{ij} I^2 \right] m_j \quad (\text{A-10})$$

where  $A$  is the Debye-Hückel coefficient which depends on temperature and solvent properties,  $z_i$  is the number of charges on ion  $i$ ,  $I$  is the ionic strength (i.e.,  $I = 0.5 \sum z_i^2 m_i$ ),  $NO$  is the number of ions with charges opposite to that of ion  $i$ , and  $B_{ij}$ ,  $C_{ij}$  and  $D_{ij}$  are empirical, temperature-dependent cation-anion interaction parameters. Bromley's<sup>41</sup> original formulation contains only one interaction parameter,  $B_{ij}$ , which is sufficient for systems with moderate ionic strength. For concentrated systems, the two additional coefficients  $C_{ij}$  and  $D_{ij}$  usually become necessary. The three-parameter form of the Bromley model is capable of reproducing activity coefficients in solutions with ionic strength up to 30 mol/kg. The temperature dependence of the  $B_{ij}$ ,  $C_{ij}$  and  $D_{ij}$  parameters is usually expressed using a simple quadratic function.

The Bromley model is restricted to interactions between cations and anions. For ion-molecule and molecule-molecule interactions, the well-known model of Pitzer<sup>42</sup> is used. To calculate the fugacities of components in the gas phase, the Redlich-Kwong-Soave<sup>43</sup> equation of state is used.

In the absence of sufficient experimental data, reasonable predictions can be made using a method due to Meissner<sup>44</sup>, which makes it possible to extrapolate the activity coefficients to higher ionic strengths based on only a single, experimental or predicted, data point.

## APPENDIX B: CALCULATION OF THE MASS TRANSFER COEFFICIENT

The mass transfer coefficient  $k_m$  (eq. 13) can be calculated once the flow geometry is assumed. For a rotating disk, the equation of Levich<sup>45</sup> holds:

$$k_m = 0.62 D^{2/3} \nu^{-1/6} \omega^{1/2} \quad (\text{B-1})$$

where  $D$  is the diffusion coefficient of the species that undergoes the electrode reaction,  $\nu$  is the kinematic viscosity and  $\omega$  is the rotation velocity. The diffusion coefficient and viscosity are calculated as functions of temperature and concentration using the methods developed by Anderko and Lencka<sup>7</sup> and Lencka et al.<sup>6</sup>, respectively.

For straight pipe and rotating cylinder geometry, the mass transfer coefficient can be expressed in terms of the dimensionless Reynolds ( $Re$ ) and Schmidt ( $Sc$ ) numbers. These numbers are defined by:

$$Re = \frac{vd}{\nu} \quad (\text{B-2})$$

$$Sc = \frac{\nu}{D} \quad (\text{B-3})$$

where  $v$  is the linear velocity and  $d$  is the diameter. For single-phase flow in a straight pipe, the correlation of Berger and Hau<sup>46</sup> can be used, i.e.,

$$\frac{k_m d}{D} = 0.0165 Re^{0.86} Sc^{0.33} \quad (\text{B-4})$$

For a rotating cylinder, the correlation of Eisenberg et al.<sup>47</sup> applies, i.e.,

$$\frac{k_m d}{D} = 0.0791 Re^{0.70} Sc^{0.356} \quad (\text{B-5})$$